

# Generalized Disturbance Estimation via ESLKF for the Motion Control of Rotorcraft Having a Rod-suspended Load

J. Escareno<sup>1,2</sup>, A. Belbachir<sup>1</sup>, T. Raharijaona<sup>3</sup> and S. Bouchafa<sup>2</sup>

<sup>1</sup>*Institut Polytechnique des Sciences Avancées, 194200 Ivry sur Seine, France*

<sup>2</sup>*Université d'Evry, Laboratoire IBISC, 91020 Evry, France*

<sup>3</sup>*Aix-Marseille Université, CNRS, ISM UMR 7287, 13288 Marseille Cedex 09, France*

**Keywords:** Multi-body Rotorcrafts, Linear Kalman Filter, Extended-state Estimation, Robust Navigation, Hierarchical Control, Time-scale Separation.

**Abstract:** The aim of the paper is to propose a navigation strategy applied to a class of rotorcraft having a free rod-suspended load. The presented approach relies on the Linear Kalman Filter to estimate the not only the state vector but also a generalized disturbance term containing parametric, couplings and external uncertainties. A simple hierarchical control is used to drive the motion of the rotorcraft, which is thus updated with the estimation of the disturbance evolving during the a navigation task. Despite the time-scale separation due to the underactuated nature of the flying robot, the estimation approach has shown its effectiveness considering the same sampling time. A detailed simulation model is used to evaluate the performance of the proposal under different disturbed scenarios.

## 1 INTRODUCTION

In the last years the Unmanned Aerial Vehicles (UAVs), specially miniature aerial vehicles (MAVs) were used for a wide variety of tasks either industrial or scientific. The operational capabilities of these aerial vehicles are evolving and thus novel applications are arising. The technological and scientific challenges associated to this emergent generation of aerial robots are enormous. The aerial interactivity with the environment is a trendy MAV-based applications category, whose most notorious examples are in-contact structure inspection, aerial manipulation and transportation.

The dynamic structure of a rotorcraft endowed with a rod-suspended load, either rigidly attached to airframe (robotic arm) or freely rotating pendulum (rod cable-suspended load), can be considered as a general case for aerial manipulation and transportation. Several works have been proposed in such topics. In (Bernard et al., 2010), the problem of slung load transportation using autonomous small size helicopters is addressed. The Newton-Euler modeling and control of a variable number of helicopters transporting a load is presented. Indeed, the proposed controller prevents and compensates oscillations of load during the flight, which is demonstrated by real

flight load transportation by three helicopters. On the other hand in the case of rotorcrafts mini aerial vehicles (MAVs), they features a reduced payload-carrying capacity which represents an critical issue while transporting cargo or aerial grasping. However, multiple vehicles are able to overcome this issue, as demonstrated (Mellinger et al., 2010), where a quad-rotors fleet transport a cargo through cables. The generation of trajectories where the quadrotor provides swing-free load motion has attracted the interest of diverse authors. In (Palunko et al., 2012) is presented the strategy to generate trajectories that provides a swing-free load's motion. In (Faust et al., 2013) the same problem is addressed using a reinforcement learning algorithm to reduce loads oscillations. Sharing the same objective, in (Cruz and Fierro, 2014) a geometric control is proposed. An alternative UAV configuration equipped with a hook intended to deliver/retriving cargo using a vision-based strategy is presented in (Kuntz and Oh, 2008). Likewise, various contributions can be found on the literature regarding the aerial grasping and/or manipulation. (Pounds et al., 2011) presents the planar model, attitude control analysis and outdoors experimental validation of a middle-size helicopter equipped with a compliant gripper capable of robust grasping and transporting objects of different shapes and dimensions. In (Gha-

diok and Ren, 2012), a classical quadrotor featuring a home-customized 1DOF gripper performs an aerial grasping based IR camera. In (Ghadiok and Ren, ), the experiments are extended to outdoor, using a GPS system and a Kalman filter to improve the precision in the position system. Both contributions use a customized 1-DOF gripper. (Yeol and Lin, 2014) presents a quadrotor equipped with a four-fingered gripper which enables to perform aerial grasping and perching. The gripper is directly attached to the vehicle, this fact restricts the grasping workspace, i.e. the vehicle's center of mass (CoM) must be aligned to the object to be grasped (target). From the mechanical point of view, the gripper is significantly complex featuring 16 DOF, 4 joints per finger. In (Thomas et al., 2014), the authors present a classical quadrotor equipped with a monocular camera. The proposed control strategy enables performing aggressive grasping maneuvers via an Image Based Visual Servoing (IBVS). It is claimed that unlike most IBVS approaches, the dynamics is obtained directly in the image to deal with a second order system. In (Pizetta et al., 2015) it is presented the modeling and bounded control of a quadrotor having a suspended load. In this case the dynamic couplings are considered only in the translational subsystem of the aerial robot, and the pitch dynamics lacks of dynamic couplings. This simplifies the control task since the underactuated nature of the overall rotorcraft's motion relies on the pitch control effectiveness.

While most of the contributions, related with suspended load, focuses on the trajectory generation to attain a swing-free motion, in the current paper we prioritize the navigation stability of the rotorcraft regardless the dynamic disturbances resulting from the coupling with the motion of a freely rotating pendulum (aerial pendulum) which is also vulnerable to external disturbances, which. The paper provides a detailed description of the dynamic model, which is obtained through the Euler-Lagrange formalism. The rotorcraft model is represented as disturbed system, affected by the couplings with aerial pendulum. We have based our estimation approach on the Linear Kalman Filter (LKF), whose framework allows to define extended states to take into account the unknown inputs. In this regard, the LKF is applied in both dynamic layers, the rotational and translational, which feature a nonlinear underactuated dynamic structure. Despite the time-scale separation between such dynamics, the LKF is implemented considering the same sampling-time.

The paper is organized as follows. Section 1 describe the context and previous works of the herein presented rotorcraft class the grasping problem is dis-

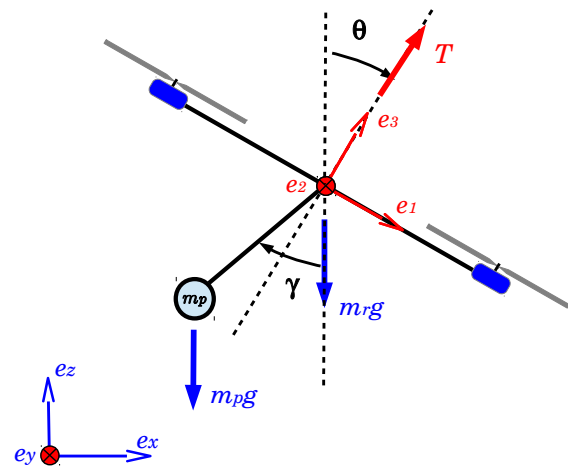


Figure 1: Drone Pendulum.

cussed. Section 2 details the mathematical model obtained via the Euler-Lagrange. Section 3 and 4, describes the navigations strategy. Finally, section 5 provides the conclusions and future works.

## 2 DYNAMIC MODEL

Consider a rotorcraft, of mass  $m_r \in \mathbb{R}$ , having a load mass  $m_p \in \mathbb{R}$  which is linked to the main airframe through a massless rigid rod of length  $l_p \in \mathbb{R}$  (aerial pendulum). For the actual study and for the sake of simplicity, the rotorcraft is restricted to evolve within the longitudinal plane (see Fig.2). For such class of vehicle, the general expressions that governs the dynamic behavior are obtained through the Euler-Lagrange approach, such energy-based formalism provides cross-linked couplings between the rotorcraft and the payload. Let  $\theta \in \mathbb{R}$  represent the pitch angle,  $\gamma \in \mathbb{R}$  the rod's angle with respect to (w.r.t.)  $-e_3$ , while  $T_1$  and  $T_2$  denote the thrust force provided by frontal and rear propellers, respectively. The inertial frame is denoted by  $\{I : (e_x, e_y, e_z)\}$  and the body-fixed frame is  $\{B : (e_1, e_2, e_3)\}$  and the rotation matrix relating the body frame with inertial is  $\mathcal{R}^\theta \in SO(3)$  which corresponds and is given as The equations of motion modeling a rotorcraft having a free pendular mass represent a versatile model that can be adapted or simplified for several multi-body rotorcraft configurations. For instance, the current trend of flying robots featuring actuated robotic manipulators can be considered as a vehicle sub-class of the rod-load configuration. In this regard, diverse nonlinear adverse terms, coupling and external disturbances, arise during in-hovering grasping, manipulation and surface-contact operations, affecting the nominal moments and forces equations. Furthermore,

couplings arise from translational motion and, obviously, due to vehicle's underactuated nature, the rotational motion.

In order to obtain the equations of motion through the Euler-Lagrange, it is required the knowledge of the kinetic and potential energies for the rotorcraft and the rod-load mechanisms.

## 2.1 Kinetic Energy

The kinetic energy function of the rotorcraft is given,

$$K_r = \frac{1}{2}I_r\dot{\theta}^2 + \frac{1}{2}m_r\dot{x}^2 + \frac{1}{2}m_r\dot{z}^2. \quad (1)$$

where  $I_r$  denotes the inertia tensor of the rotorcraft. Due coordinates of the pendular mass are shifted from the body frame  $\mathcal{B}$ , the kinetic energy of aerial pendulum is written

$$K_p = \frac{1}{2}m_p\dot{x}_p^2 + \frac{1}{2}m_p\dot{z}_p^2 \quad (2)$$

where  $m_p$  represents the pendular mass, and

$$\begin{aligned} \dot{x}_p &= \dot{x} - l_p\dot{\gamma}\cos\gamma \\ \dot{z}_p &= \dot{z} + l_p\dot{\gamma}\sin\gamma \end{aligned}$$

are obtained from the cartesian coordinates follow a right-handed rotation about  $e_2$

$$\begin{aligned} x_p &= x - l_p\sin\gamma \\ z_p &= z - l_p\cos\gamma \end{aligned}$$

Thus, the expression for the aerial pendulum is written as

$$K_p = \frac{1}{2}m_p(\dot{x} - l_p\dot{\gamma}\cos\gamma)^2 + \frac{1}{2}m_p(\dot{z} + l_p\dot{\gamma}\sin\gamma)^2. \quad (3)$$

It is straightforward to reduce latter equation into

$$K_p = \frac{1}{2}m_p\dot{x}^2 + \frac{1}{2}m_p\dot{z}^2 + \zeta_c(\dot{x}, \dot{z}, \dot{\gamma}) + \frac{1}{2}m_pI_p\dot{\gamma}^2, \quad (4)$$

where  $\zeta_c$  energy coupling and is given

$$\zeta_c = m_p l_p \dot{\gamma} (-\dot{x} \cos\gamma + \dot{z} \sin\gamma). \quad (5)$$

The total kinetic of the aerial multi-body system is

$$K = K_r + K_p \quad (6)$$

## 2.2 Potential Energy

The potential energy of the of the rotorcraft is obtained as

$$P_r = m_r g z \quad (7)$$

while that of the aerial pendulum is written as

$$P_p = m_p g (z - l_p \cos\gamma) \quad (8)$$

The total potential energy is

$$P = P_r + P_p \quad (9)$$

## 2.3 Equations of Motion

The Lagrangian  $\mathcal{L} \in \mathbb{R}$  is  $\mathcal{L} = K - P$ . Hence, in order to obtain the equations of motion, the general Euler-Lagrange equation is solved for the different generalized coordinates  $q = (x, z, \theta, \gamma)^T \in \mathbb{R}^4$

$$\frac{d}{dt} \left( \frac{\partial \mathcal{L}}{\partial \dot{q}} \right) - \frac{\partial \mathcal{L}}{\partial q} = U, \quad (10)$$

where the control inputs vector  $U = (u_x, u_z, u_\theta, u_\gamma)^T = (U_t, U_r)^T$ . For the underactuated translational motion subsystem, the rotational matrix angles the thrust vector  $T$  as

$$U_t = \mathcal{R}^\theta T e_3 = (T \sin\theta, T \cos\theta)^T = (u_x, u_z)^T \quad (11)$$

is the thrust vectoring through pitch angle. Concerning, the rotational motion control input,

$$U_r = (u_\theta, u_\gamma)^T, \quad (12)$$

one can notice that unlike rotorcraft's attitude the aerial pendulum is not actuated (i.e.  $u_r = 0$ ).

The equations of motion results from solving Eq.10 for the different generalized coordinates. For the translational motion, we obtain

$$(m_r + m_p)\ddot{x} - m_p l_p \ddot{\gamma} \cos\gamma + m_p l_p \dot{\gamma}^2 \sin\gamma = u_x \quad (13)$$

$$(m_r + m_p)\ddot{z} + m l_p \ddot{\gamma} \sin\gamma + m_p l_p \dot{\gamma}^2 \cos\gamma + (m_r + m_p)g = u_z \quad (14)$$

The corresponding equations describing the rotational motion of the rotorcraft and the aerial pendulum are given next.

$$I_r \ddot{\theta} = u_\theta \quad (15)$$

and

$$m_p l_p^2 \ddot{\gamma} - m_p l_p \ddot{x} \cos\gamma + \ddot{z} m_p l_p \sin\gamma + m_p g l_p \sin\gamma = u_\gamma \quad (16)$$

where  $u_\gamma = 0$  since the aerial pendulum is in free motion.

**Remark 2.1.** *It is important to point out that the torques of the pendulum dynamics are also exerted about the axis  $e_2$  as the pitch dynamics. Thus, pitch behavior is also impacted by the pendulum's torques*

## 2.4 Disturbed System

The equations (Eq.13-Eq.16) obtained from the Euler-Lagrange formulation (Eq.10), are rewritten in order to represent coupled system as disturbed system. In this representation, the coupling terms are considered as disturbances since they are assumed unknown. In this regard, the mass of the pendulum is unknown but verifying

$$m_p < m_r \quad (17)$$

The equations describing the horizontal motion are rewritten as follows:

$$\ddot{x} = \frac{1}{m_r}(u_x + \rho_x), \quad (18)$$

with

$$\rho_x = -m_p \ddot{x} + m_p l_p \ddot{\gamma} \cos \gamma - m l_p \dot{\gamma}^2 \sin \gamma \quad (19)$$

whereas, the vertical motion is rewritten as

$$m_r \ddot{z} = \frac{1}{m_r}(u_z + \rho_z) - g, \quad (20)$$

with

$$\rho_z = -m_p \ddot{z} - m_p l_p \ddot{\gamma} \sin \gamma - m_p l_p \dot{\gamma}^2 \cos \gamma - m_p g \quad (21)$$

One can notice that  $\rho_x$  and  $\rho_z$  corresponds to the tangential, centrifugal and gravity-due forces generated by the pendular motion of the mass  $m_p$ . Even if the torques of the rotorcraft and aerial pendulum are exerted about the  $e_2$  axis, the rotational motion of the of the aerial pendulum is not affected (assuming  $\mu = 0$ ) by that of the rotorcraft. However, this is not the case for the rotorcraft rotational motion, which is affected by the torques due the motion of the pendular motion shifting the center of gravity of the rotorcraft. The latter allows us to rewrite the rotorcraft dynamics Eq.15 as:

$$\ddot{\theta} = \frac{1}{I_r}(u_\theta + \rho_\theta) \quad (22)$$

with

$$\rho_\theta = -m_p l_p \ddot{\gamma} + m_p l_p \ddot{x} \cos \beta - \ddot{z} m_p l_p \sin \beta - m_p g l_p \sin \gamma \quad (23)$$

### 3 DISTURBANCE ESTIMATION STRATEGY

An extended state discrete linear Kalman filter (ESLKF) is designed regarding the estimation of the couplings and disturbances arising during a planar displacement at rotational (inner dynamics) and translational (external dynamics) The Linear Kalman Filter (LKF) is derived from a continuous system

$$\begin{cases} \dot{x}(t) = Ax(t) + Bu(t) + \mathcal{M}\omega(t) & \rightarrow \text{process} \\ y(t) = Cx(t) + v(t) & \rightarrow \text{sensor(s)} \end{cases} \quad (24)$$

that considers the following hypothesis:

- H1. The pair AC verifies the controllability property
- H2. The signals  $\alpha$  and  $\beta$  stand for a white Gaussian random process with zero-mean ( $E[\alpha(t)] = 0$  and  $E[\beta(t)] = 0$ ) with constant power spectral density (PSD)  $W(t)$  and  $V(t)$  defining respectively:

- The process covariance matrix

$$Q = E[\alpha(t)\alpha(t+\tau)^T] = W\Delta(\tau) \quad (25)$$

- The sensor covariance matrix

$$R = E[\beta(t)\beta(t+\tau)^T] = V\Delta(\tau) \quad (26)$$

It is also assumed that both stochastic processes are not correlated, i.e.

$$E[\alpha(t)\beta(t)^T] = 0 \quad (27)$$

#### 3.1 Extended-state Estimation Strategy

Since we are interested in the stability of the rotorcraft The kalman filter is applied to the rotorcraft. Let us regroup the set of scalar disturbed systems Equ. 18, Equ. 20 and Equ. 22.

$$\ddot{\chi}_i = \frac{1}{a_i}(U_i + \rho_i) - G_i \text{ with } i \in \{x, z, \theta\} \quad (28)$$

with

- $G_x = 0, G_z = g$  and  $G_\theta = 0$
- $\ddot{\chi}_x = \ddot{x}, \ddot{\chi}_z = \ddot{z}$  and  $\ddot{\chi}_\theta = \ddot{\theta}$
- $a_x = m_r, a_z = m_r$  and  $a_\theta = I_r$

In Equ. 28 we have included the  $G_i$  term to keep the general  $i$ -structure regrouping the three disturbed dynamics. The model Equ. 28 may be rewritten into the space-state representation

$$\begin{aligned} \dot{X} &= AX + B(u_i - a_i G_i) + P\rho_i \\ Y &= CX \end{aligned} \quad (29)$$

having as a state and output vector

$$X = Y = (\chi_i, \dot{\chi}_i)^T = (\chi_{1i}, \chi_{2i})^T \quad (30)$$

the latter indicates that translational and rotational positions and velocities are available. The vector  $\rho_i$  unifies the couplings and external disturbances. The matrices of the system (Equ. 29) are given by:

$$A = \begin{pmatrix} 0 & 1 \\ 0 & 0 \end{pmatrix}, B = \begin{pmatrix} 0 \\ a_i \end{pmatrix}, P = \begin{pmatrix} 0 \\ a_i \end{pmatrix}, C = \begin{pmatrix} 1 & 0 \\ 0 & 1 \end{pmatrix}, \quad (31)$$

It is assumed that no prior information about the disturbance is available. However, we consider that the disturbance has a slow time-varying dynamics that can be modeled by a random walk process

$$\dot{\rho}_i = \omega(t) \text{ with } i \in \{x, z, \theta\} \quad (32)$$

with  $\omega(t)$  defined by **H2**. The latter assumption allows us to introduce an extended state-space vector:

$$X^e(t) = (\chi_i, \dot{\chi}_i, \rho_i)^T \quad (33)$$

and its associated state-space model describing the dynamics is obtained from (Equ. 32) in which the unknown input disturbance  $\rho_i(t)$  is incorporated in the state transition matrix:

$$\dot{X}^e(t) = \mathcal{A}X^e(t) + \mathcal{B}(U_i - a_i G_i) + \mathcal{M}\alpha_i \quad (34)$$

$$Y^e(t) = CX^e(t) + \beta_i \quad (35)$$

with

$$\mathcal{A} = \begin{pmatrix} 0 & 1 & 0 \\ 0 & 0 & \frac{1}{a_i} \\ 0 & 0 & 0 \end{pmatrix} \quad \mathcal{B} = \begin{pmatrix} 0 \\ \frac{1}{a_i} \\ 0 \end{pmatrix} \quad (36)$$

$$\mathcal{M} = \begin{pmatrix} 0 \\ 0 \\ 1 \end{pmatrix} \quad C = \begin{pmatrix} 1 & 0 & 0 \\ 0 & 1 & 0 \end{pmatrix} \quad (37)$$

The continuous-time model (Equ. 38) can be discretized with sampling time  $T_s$ . Assuming zero-order hold (zoh) of the input yields

$$\dot{X}_k^e = \mathcal{A}_k X_k^e + \mathcal{B}_k (U_{i_k} - a_i G_{i_k}) + \mathcal{M}\alpha_{i_k} \quad (38)$$

$$Y_k^e = C_k X_k^e + \beta_{i_k} \quad (39)$$

with

$$X_k^e = (\chi_{i_k}, \dot{\chi}_{i_k}, \rho_{i_k})^T \quad (40)$$

$$\mathcal{A}_k = e^{\mathcal{A}T_s} \quad (41)$$

$$\mathcal{B}_k = \left( \int_0^{T_s} e^{\mathcal{A}T_s} \mathcal{B} dt \right) \quad (42)$$

$$\alpha_{i_k} = (\alpha_k^{\chi_{i_k}}, \alpha_k^{\dot{\chi}_{i_k}}, \alpha_k^{\rho_{i_k}})^T \quad (43)$$

$$\beta_{i_k} = (\beta_k^{\chi_{i_k}}, \beta_k^{\dot{\chi}_{i_k}}) \quad (44)$$

where  $\alpha_k$  and  $\beta_k$  are discrete-time band-limited white gaussian random process with zero-mean characterizing uncertainties on the model (unmodeled dynamics and parametric uncertainties) and measurement (noisy sensors) equations, respectively.

The model uncertainties discrete covariance matrix  $Q_k$  is:

$$Q_k = E [\alpha_k \alpha_k^T] = \int_0^{T_s} e^{\mathcal{A}t} \mathcal{M} Q \mathcal{M}^T e^{\mathcal{A}^T t} dt \quad (45)$$

being the process covariance matrix

$$Q = \text{diag} [\sigma^2(\chi_{i_0}), \sigma^2(\dot{\chi}_{i_0}), \sigma^2(\rho_{i_0})] \quad (46)$$

The classical LKF is very attractive for experimental applications due to its simplicity and low computational demand. The algorithm that computes the estimate (including the disturbance  $\rho_i$ ) of the state vector  $X_k^e$  is initialized as follows:

- The initial scenario for the extended system is assumed to be at the equilibrium state, i.e.

$$x_{i_0}^e = (0, 0, 0)^T \quad (47)$$

- The initial covariance matrix  $P_0$  is considered as

$$P_0 = \text{diag} [\sigma^2(\chi_{i_0}), \sigma^2(\dot{\chi}_{i_0}), \sigma^2(\rho_{i_0})] \quad (48)$$

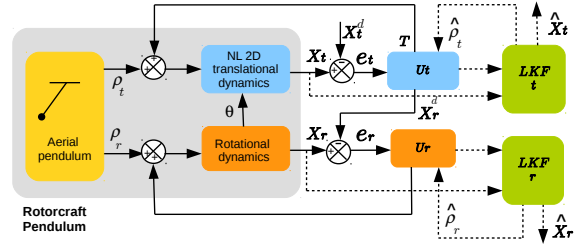


Figure 2: Closed-loop architecture.

The corresponding LKF recursive algorithm features a prediction-estimation structure and is provided next

Prediction stage

$$\hat{x}_{est_k} = \mathcal{A}_k \hat{x}_{est_{k-1}} + \mathcal{B}_k u_k$$

$$P_{pred_k} = \mathcal{A}_k P_{est_{k-1}} \mathcal{A}_k^T + Q$$

$$K_k = P_{pred_k} C_k^T (C_k P_{pred_k} C_k^T + R)^{-1}$$

Estimation stage

$y_k$  = measurement vector

$$\hat{x}_{est_k} = \hat{x}_{pred_k} + K_k (y_k - C_k \hat{x}_{pred_k})$$

$$P_{est_k} = (I - K_k C_k) P_{pred_k} (I - K_k C_k)^T$$

where  $K_k$  denotes the Kalman filter gain, and  $I$  is the identity matrix. The estimated vector state generated by the LKF is the written:

$$\hat{x}_k^e = (\hat{\chi}_{i_k}, \hat{\dot{\chi}}_{i_k}, \hat{\rho}_{i_k})^T \quad (49)$$

For the actual work it was considered

$$\hat{\rho}_{i_k} = C_d \hat{x}_k^e \quad (50)$$

with  $C_d = (0, 0, 1)^T$

## 4 CONTROL WITH LKF-BASED DISTURBANCE COMPENSATION

Based on the dynamic model Equ.28, let the control input  $U_i$  in Equ.28 of the translational be

$$u_i = \frac{1}{a_i} (v_i - \hat{\rho}_i) + G_i \quad (51)$$

where it is assumed the knowledge of the disturbance, through the estimation coming from the LKF. The previous equation Equ.51 is twofold, featuring a control input for an actuated dynamics (attitude) and an underactuated dynamics (translational motion), where the attitude dynamics drives the translational behavior of the flying robot. Therefore, let the control input for the actuated dynamics be

$$u_{\theta} = I(v_{\theta} - \hat{\rho}_{\theta}), \quad (52)$$

with

- $v_\theta = k_{p_\theta} e_\theta + k_{d_\theta} \dot{e}_\theta$  with  $e_\theta = \theta - \theta^d$

On the other hand, let the control input for the translational motion be

$$(u_x, u_z)^T = \mathcal{R}^\theta T e_3 = \frac{1}{a_j} (v_j - \hat{p}_j) + G_j \text{ with } j \in \{x, z\} \quad (53)$$

with

- $v_x = k_{p_x} e_x + k_{d_x} \dot{e}_x$  with  $e_x = x - x^d$
- $v_z = k_{p_z} e_z + k_{d_z} \dot{e}_z$  with  $e_z = z - z^d$

This allows to consider that the classical terms for the desired thrust and attitude, i.e.

$$T^d = \left\| \begin{bmatrix} u_x \\ u_z \end{bmatrix} \right\| \text{ and } \theta^d = \tan^{-1} \left( \frac{u_x}{u_z} \right) \quad (54)$$

The overall control input  $u_i$ , assuming an effective disturbance estimation, leads to

$$u_i = v_i \quad (55)$$

providing exponential stability.

**Remark 4.1.** The control input (Eq.54) used to linearize the system the translational subsystem (Eq.53) admits pitch displacements of  $|\theta| < \frac{\pi}{2}$

## 5 NUMERICAL SIMULATIONS

This section presents the simulation results carried out to evaluate the effectiveness of the actual control-estimation strategy to drive the rotorcraft according a desired reference regardless the motion of the rod-suspended load.

The parameters used to simulate the aerial robot are depicted in table 1

The parameters of the ES-LKF are presented in table

### 5.1 Regulation Task

The main goal is to solve a regulation problem, having  $x^d = 8[m]$  and  $z^d = 3[m]$ . A first set of tests are provided to show the performance of the system without/with the disturbance compensation either in

Table 1: Simulation parameters.

Parameter	value
$m_r$	$0.5[Kg]$
$m_p$	$m_r/4[Kg]$
$l_p$	$0.35[m]$
$I_r$	$0.177$
$I_m$	$m_p l_p^2$

the translational and rotational subsystem. In this regard, an external disturbance is applied in the rotational subsystem to observe the consequences when the center of gravity shifts away.

- The behavior of the rotorcraft when the coupling disturbance are not compensates is depicted on Fig.3.
- The states behavior using the estimated disturbances is shown by Fig.4.
- Following a progressive criteria, now, let us show the behavior of the rotorcraft, with and without disturbance compensation, while a sudden torque disturbance is exerted on the aerial pendulum at  $t = 15[sec]$ . Such scenario is presented by Fig.5, Fig.6

### 5.2 Trajectory Tracking Task

In this part of the paper, the commanded reference is modified in order to appreciate the effectiveness of the proposed approach while tracking a circular trajectory  $x^d(t) = 4 \sin(2\pi ft)$  and  $z^d(t) = 4 \cos(2\pi ft)$ . The torque disturbance appearing at  $t = 15[sec]$  is still considered. The behavior of the rotorcraft while following a trajectory without and with compensation is displayed by Fig.7, Fig.8, Fig.9 and Fig.10

Table 2: Kalman Filter parameters. We have also added a noise to sensor outputs whose variance value is  $R_i = 1e-3$ .

Parameter	value
$T_{samp}$	$0.01[S]$
$Q_{x_{11}}/Q_{x_{22}}/Q_{x_{33}}$	$0/0/1$
$Q_{z_{11}}/Q_{z_{22}}/Q_{z_{33}}$	$0/0/1$
$Q_{\theta_{11}}/Q_{\theta_{22}}/Q_{\theta_{33}}$	$0/0/1$
$l_p$	$0.35[m]$
$I_r$	$0.177$
$I_m$	$m_p l_p^2$

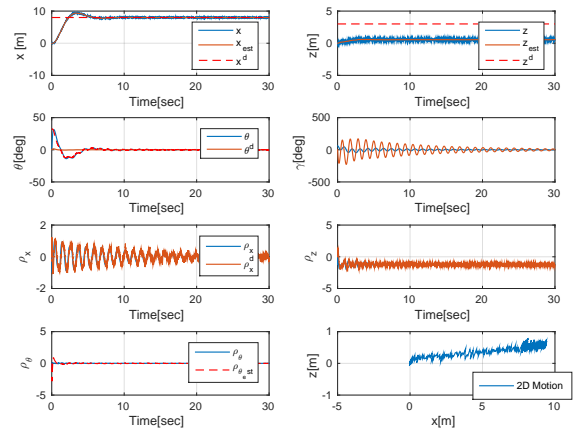


Figure 3: States evolution during a regulation task without disturbance compensation.

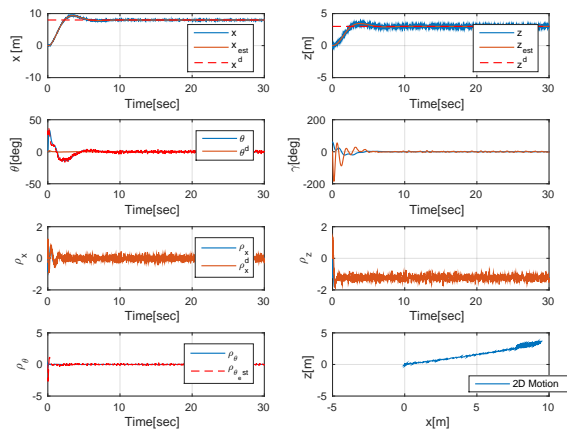


Figure 4: States evolution during a regulation task with disturbance compensation.

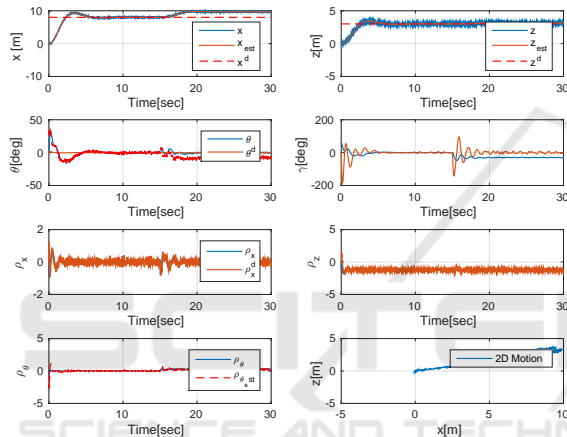


Figure 5: States behavior without the disturbance compensation in the rotational layer.

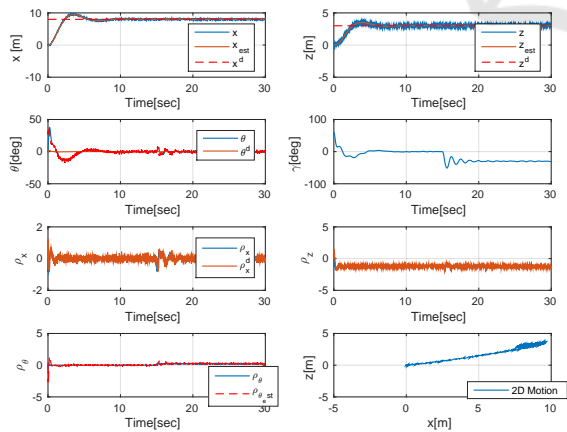


Figure 6: States behavior with the disturbance compensation in the rotational layer.

## 6 CONCLUDING REMARKS

The paper has presented a navigation strategy using an extended-state LKF-based disturbance estima-

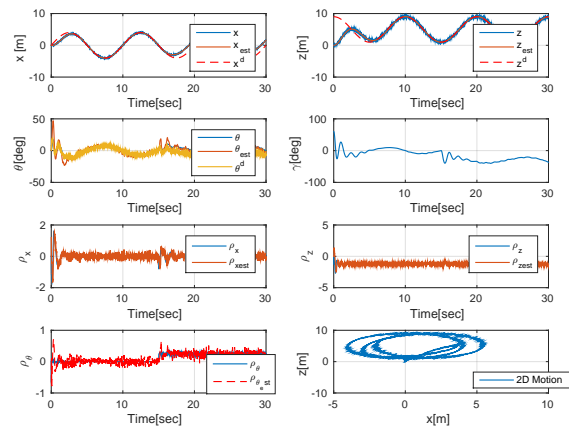


Figure 7: States behavior without the disturbance compensation in the rotational layer.

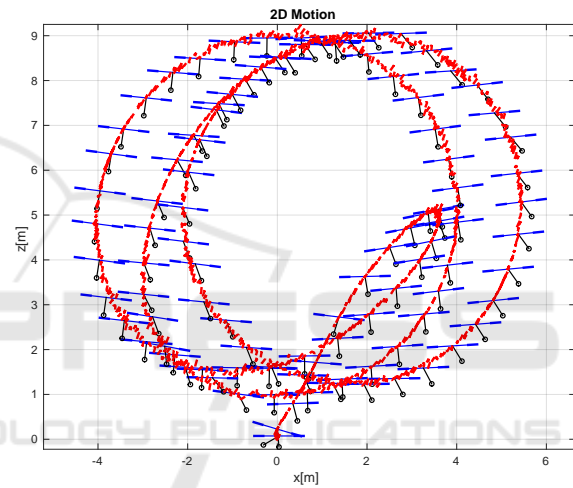


Figure 8: 2D motion without the disturbance compensation in the rotational layer.

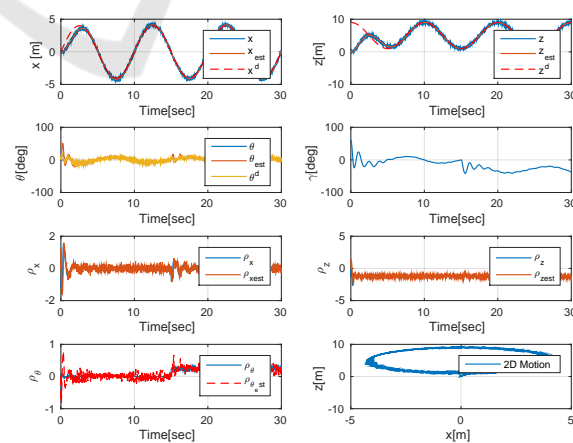


Figure 9: States behavior with the disturbance compensation in the rotational layer.

tion combined with a simple two-time scale control scheme. Despite the time-scale separation between dynamics, the structure of LKF is shared by the trans-

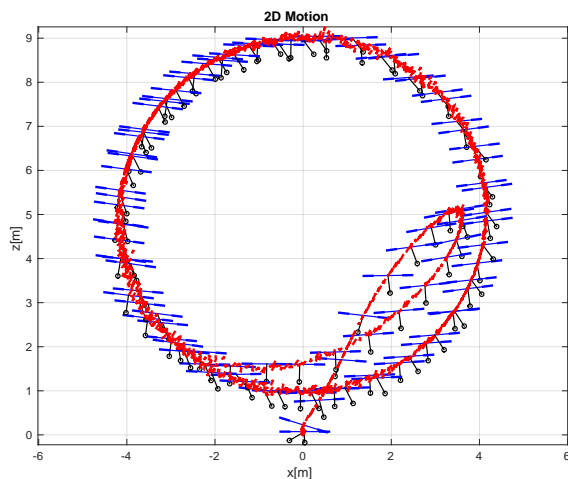


Figure 10: 2D motion with the disturbance compensation in the rotational layer.

lational and rotational dynamic layers, i.e. it uses the same sampling time. The approach has shown its effectiveness in two scenarios where the couplings have a significant adverse effect on the overall performance, either for a simple regulation or trajectory tracking tasks. The modularity of the approach will allow to extend the approach to the 3D case under windy conditions.

## REFERENCES

- Bernard, M., Kondak, K., and Hommel, G. (2010). Load transportation system based on autonomous small size helicopters. *Aeronautical Journal*, 114(1153):191–198.
- Cruz, P. and Fierro, R. (2014). Autonomous lift of a cable-suspended load by an unmanned aerial robot. In *2014 IEEE Conference on Control Applications (CCA)*, pages 802–807.
- Faust, A., Palunko, I., Cruz, P., Fierro, R., and Tapia, L. (2013). Learning swing-free trajectories for uavs with a suspended load. In *Robotics and Automation (ICRA), 2013 IEEE International Conference on*, pages 4902–4909.
- Ghadiok, V., G. J. and Ren, W. On the design and development of attitude stabilization, vision-based navigation, and aerial gripping for a low-cost quadrotor.
- Ghadiok, V., G. J. and Ren, W. (2012). Autonomous indoor aerial gripping using a quadrotor. In *2011 IEEE/RSJ International Conference on Intelligent Robots and Systems*.
- Kuntz, N. R. and Oh, P. Y. (2008). Towards autonomous cargo deployment and retrieval by an unmanned aerial vehicle using visual servoing. In *ASME 2008 International Design Engineering Technical Conferences and Computers and Information in Engineering Conference*, pages 841–849. American Society of Mechanical Engineers.
- Mellinger, D., Shomin, M., and Kumar, V. (2010). Control of quadrotors for robust perching and landing. In *Proceedings of the International Powered Lift Conference*, pages 205–225.
- Palunko, I., Fierro, R., and Cruz, P. (2012). Trajectory generation for swing-free maneuvers of a quadrotor with suspended payload: A dynamic programming approach. In *IEEE International Conference on Robotics and Automation (ICRA) 2012*, pages 2691–2697.
- Pizetta, I. H. B., Brando, A. S., and Sarcinelli-Filho, M. (2015). Modelling and control of a pvtol quadrotor carrying a suspended load. In *Unmanned Aircraft Systems (ICUAS), 2015 International Conference on*, pages 444–450.
- Pounds, P. E., Bersak, D., and Dollar, A. (2011). Grasping from the air: Hovering capture and load stability. In *Robotics and Automation (ICRA), 2011 IEEE International Conference on*, pages 2491–2498.
- Thomas, J., Loianno, G., Sreenath, K., and Kumar, V. (2014). Toward Image Based Visual Servoing for Aerial Grasping and Perching. In *ICRA. IEEE*.
- Yeol, J. W. and Lin, C.-H. (2014). Development of multi-tentacle micro air vehicle. In *Unmanned Aircraft Systems (ICUAS), 2014 International Conference on*, pages 815–820.